

Non-hexagonal-ring defects and structures induced by strain in graphene and in functionalized graphene

Joice da Silva-Araújo, A. J. M. Nascimento, Hélio Chacham, and R. W. Nunes*
*Departamento de Física, Universidade Federal de Minas Gerais,
 CP 702, 30123-970, Belo Horizonte, MG, Brazil*

We perform *ab initio* calculations for the strain-induced formation of non-hexagonal-ring defects in graphene, graphane (planar CH), and graphenol (planar COH). We find that the simplest of such topological defects, the Stone-Wales defect, acts as a seed for strain-induced dissociation and multiplication of topological defects. Through the application of inhomogeneous deformations to graphene, graphane and graphenol with initially small concentrations of pentagonal and heptagonal rings, we obtain several novel stable structures that possess, at the same time, large concentrations of non-hexagonal rings (from fourfold to elevenfold) and small formation energies.

PACS numbers:

I. INTRODUCTION

The intense interest in the Physics of graphene, over the last few years, derives in large part from the exceptional electronic properties of the pristine material.¹⁻⁴ While pristine samples obtained by exfoliation of graphite have allowed exploration of a rich variety of phenomena connected with the Dirac-fermion nature of the electronic excitations in graphene, current large-scale synthesis protocols have reached the point where polycrystalline or highly-inhomogeneous samples are being produced.⁵⁻⁸ In very recent experiments, graphene layers resulting from reduction of graphene oxide show conductivities that are 1 or 2 orders of magnitude smaller than those of pristine graphene,⁹⁻¹⁵ possibly due to residual dopants and intrinsic defects. Better conductivities can be obtained when partially oxidized graphene is used as a precursor.¹⁶

From the perspective of applications, widespread use of graphene will depend on the control and understanding of the properties of such defective graphene products. The atomic structure of defects in reduced graphene oxide (RGO) has been recently investigated through high resolution transmission electron microscopy (TEM)^{5,16} and molecular dynamics simulations.⁸ The experimental results show significant areas with holes, grain boundaries, isolated pentagon-heptagon pairs and clusters of carbon pentagons, hexagons, heptagons and a few octagons. Similar defect morphologies can be generated in exfoliated graphene by electron-beam irradiation,⁶ and by irradiation under extreme temperatures.⁷ The occurrence of areas with high density of extended topological defects (ETD) observed in the samples of Ref. 5 was attributed to the process of oxidation and further reduction of the graphene oxide, since such large defective areas do not appear in mechanically exfoliated graphene from the same graphite source. Moreover, in these samples residual functional groups were found to concentrate primarily on regions with ETDs, surrounded by pristine (unfunctionalized) graphene areas.

Given this current interest in defective graphene sys-

tems, in the present work, we employ *ab initio* density functional theory (DFT) calculations to study the morphological evolution of the following graphene structures: (i) homogeneously-strained graphene sheets containing a Stone-Wales (SW) defect;¹⁷ and (ii) pristine and functionalized graphene sheets containing initial distributions of isolated topological defects (TD),¹⁸ after introduction of holes and highly inhomogeneous bond deformations. We find that stress-relaxation of a graphene sheet containing SW defects may lead to the formation of ETDs, with morphological units that are very similar to those observed in the aforementioned experiments.⁵⁻⁸ We uncover the role of the SW defect as a stress-accumulation site that induces the bond rotation events which generate the ETDs. Furthermore, we find that healing of small voids coupled with the relaxation of inhomogeneously strained regions also lead to the formation of ETDs, revealing a rich variety of morphological patterns and plastic deformation mechanisms in pure and functionalized graphene structures. Our results indicate that the marked tendency of graphene to form TD clusters under strain is aided by functional groups, since the formation energies of such defective structures are considerable smaller in graphane (a graphene sheet fully functionalized with hydrogen atoms) and in graphenol (a graphene sheet fully functionalized with hydroxyl groups) than in graphene, in agreement with the experimental evidence in Ref. 5.

Our calculations are performed using Kohn-Sham density functional theory,¹⁹ the generalized-gradient approximation²⁰ for the exchange-correlation functional, and norm-conserving Troullier-Martins pseudopotentials,²¹ to describe the electron-ion interactions. We use the LCAO method implemented in the SIESTA code,²² with a double-zeta pseudo-atomic basis set augmented with polarization orbitals, with an energy cutoff of 0.01 Ry. Full structural optimization of atomic positions and supercell vectors is performed. For the relaxed structures the total force on each atom is less than 0.02 eV/Å and the pressure on the supercell is less than 1 kBar. The supercells employed are periodic along the graphene

plane, being surrounded by a 30 Å vacuum region in the transversal direction, with negligible interactions between each layer and its periodic images.

II. RESULTS AND DISCUSSION

A. Homogeneous shear deformations of graphene containing Stone-Wales defects

1. First principles results

We consider initially a likely scenario, where homogeneous shear deformations are imposed upon a graphene sheet containing a SW defect. SW defects are commonly found in graphene and nanotubes, and can be generated by irradiating the material with an 80 keV electronic beam, just below the knock-on threshold for sp^2 bonded carbon materials.^{6,23,24} The impinging electrons give out the energy needed for the 90° rotation of a carbon-carbon (C-C) bond [as indicated in Figs. 1(a) and (b)] that transforms four hexagons of the pristine graphene matrix into a SW defect. Since a SW is an incipient dislocation dipole in graphene (each pentagon-heptagon pair is one of two dislocations with opposite Burgers vectors comprising the SW defect), at first sight one expects shear deformations either to undo the C-C bond rotation and thus lead to self-annihilation of the two pentagon-heptagon pairs, or to lead to dissociation of the dislocation pair into its individual components.

In order to investigate this, we consider the two

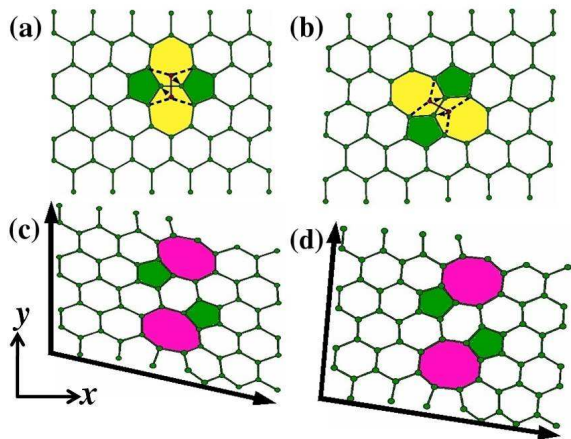


FIG. 1: Morphological transformation of a graphene sheet under strain. (a) and (b) show two images of graphene supercells containing a Stone Wales defect. The bond rotation that generates the defect is indicated. The two cases differ by the orientation of the defect with respect to the x and y axes of the cell. (c) Transformation of the supercell in (a) with relaxation of internal atomic coordinates, under homogeneous shear strain. (d) Fully-relaxed stress-free state of the structure in (c), after relaxation of cell vectors.

graphene supercells, each containing a SW defect, shown in Fig.1(a) and (b). They differ by the orientation of the SW with respect to the x and y axes of the cell (indicated in the figure). We find that a 30% shear strain of the supercell shown in Fig. 1(a) leads to the formation of the ETD shown in Figs. 1(c) and (d), containing clusters of fivefold and eightfold rings, while no morphological transformation is observed when the same deformation is imposed on the supercell shown in Fig.1(b). We shall point out that previous works have found pristine graphene to sustain deformations of up to 25% without yielding,²⁵⁻²⁷ a result that we also find in our calculations, for graphene with SW defects. The morphological pattern observed in Fig. 1(c) is obtained by allowing the system to fully relax all the internal atomic coordinates, while maintaining the imposed homogeneous strain. No further changes in morphology are observed when full relaxation of both atomic coordinates and strain (i.e. the supercell vectors) are allowed, as shown in Fig. 1(d).

These results highlight a fundamental aspect of the plastic response of a graphene sheet to imposed stresses or strains: a tendency for the formation of extended topological defects as a stress-relaxation mechanism, spawned by bond rotation events, in the above example with the formation of clusters of fivefold and eightfold rings. We note also that the transformation depends on the orientation of the shear deformation with respect to the pre-existing SW defect, that acts as stress-accumulation seed for the topological transformation.

2. Analysis of elastic energy using a Keating model

The latter point can be illustrated by following the evolution of the elastic energy of the cell during the deformation, as shown in Fig. 2. In the figure, we show a map of the elastic energy of the supercell at three different stages of the plastic relaxation process, computed using a Keating model.²⁸ Figure 2(a) shows the elastic energy for the initial strained geometry. Note that, in this configuration, the strain energy is distributed nearly uniformly over the whole system, with a larger magnitude at the SW defect. This pattern is preserved up to the point where a morphological transformation takes place. Figure 2(b) shows the strain energy right after the transformation: the important feature here is that a change in the distribution of the elastic energy takes place, from nearly uniform before the transformation to a pattern where the energy is concentrated on the ensuing ETD, and where the bulk portion of the cell relaxes to a configuration of much smaller elastic strain. Relaxation of internal atomic coordinates, after the transformation, leads to further reduction of the strain in the cell. Finally, in Fig. 2 (c) the imposed homogeneous strain is lifted and the system relaxes to a stress-free state, where the elastic energy in the bulk portions of the cell nearly vanishes, and most of the residual strain is located on the defect.

B. Deformations of graphene containing small holes and topological defects

We consider now more complex deformations of a graphene sheet, including small sized holes generated by partially ripping a graphene sheet, coupled with strongly inhomogeneous bond deformations. These can be considered a model for severely strained and ripped graphene samples, such as those obtained by reduction of GO.⁵ In the following, we show that healing of such graphene fragments, combined with relaxation of the inhomogeneous deformations, also lead to the formation of ETDs, in some cases with morphologies similar to those that have been observed in recent experiments.

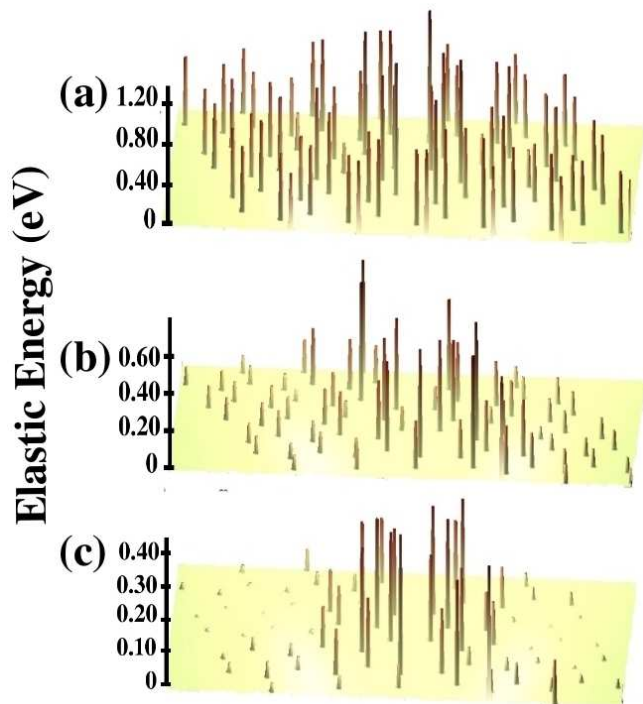


FIG. 2: Keating-energy analysis of stress relaxation by extended topological defect formation. In the initial structure a homogeneous shear strain is imposed on a graphene cell containing a Stone-Wales defect, as shown in Fig. 1(a). The location of the defect is at the top, along the center of the cell, in the regions with higher elastic-energy histogram bars. (a) In the initial structure, the elastic-strain energy is nearly uniform in both defective and bulk regions of the cell. (b) Concentration of elastic energy, after morphological transformation that generates an extended topological defect, in the process of stress relaxation under applied strain. (c) Relaxation of bulk and defect strain in the stress-free metastable structure. Most of the residual strain is located on the defect.

1. Inhomogeneous deformations of graphene containing Stone-Wales defects

We start with the supercell shown in Fig. 1(b). By imposing a homogeneous shear strain, coupled with lines of strained C-C bonds (elongated by 27% to ~ 1.8 Å) as indicated by dashed segments in Fig. 3(a) and (c), and allowing for full relaxation of both internal coordinates and homogeneous strain, the system reaches a stress-free state where the dislocation dipole is dissociated into two individual dislocations separated by a lattice constant, as shown in Fig. 3(b). When the strained bonds combine with a homogeneous shear oriented with respect to the SW defect as shown in Fig. 3(c), the SW defect induces the nucleation of an ETD consisting of two side sharing octagons connected to two pairs of pentagons, each on one of two opposite sides of the octagon pair, shown in Fig. 3(d). This ETD is similar in extent to those resulting from the 555-777 and 585 reconstructions of a divacancy in graphene.⁶

2. Inhomogeneous deformations of topological defect networks in graphene

In order to further investigate the morphologies of deformed graphene, and to access the role of functionalization and preexisting topological defects, we choose as starting configurations the three topological-defect graphene networks¹⁸ shown on the left in Fig. 4, which were labelled S_{12} , S_{31} and S_{22} in Ref. 18. We also consider the graphane²⁹ (hydrogen-functionalized) and graphenol (hydroxyl-functionalized) versions of these

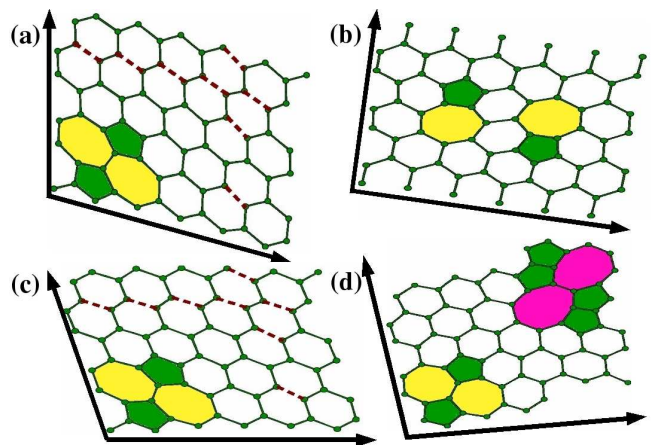


FIG. 3: Combination of homogeneous and inhomogeneous deformations of a graphene sheet: (a) and (c) show two images of homogeneously sheared supercells with a Stone Wales defect and inhomogeneous deformations generating lines of strained bonds. (b) Relaxation of the deformations in (a) leads to dislocation-dipole (Stone Wales defect) dissociation. (d) Relaxation of the deformations in (c) leads to formation of an extended topological defect.

structures, both at full coverage, with graphenol taken as a simple model for graphene oxide.³⁰ A variety of deformation patterns, including small holes, as well as compressed and/or elongated bonds were initially imposed on these structures, and each system was allowed to relax (with optimization of both atomic coordinates and supercell vectors) onto a stress-free metastable local minimum of the total-energy surface.

Figure 4 shows starting configurations before and after introduction of holes and inhomogeneous compressions, and the resulting relaxed ETD configuration. In our calculations, these are, respectively, the lowest-energy ETD for each of the following three cases: (a) pristine graphene, (b) graphane, and (c) graphenol. The two functionalized cases in Figs. 4(b) and (c) show the formation of a morphological pattern in the shape of a flower, where a square ring is surrounded by four heptagons, with pentagons connected at the perimeter. In the case of pristine graphene, the lowest-energy ETD we obtained in our calculations contains pentagon-heptagon clusters connected to pentagon-octagon units of the same morphology as the one that has been recently observed as the periodic unit of a domain-boundary in a graphene layer deposited on a nickel substrate.^{31–33}

Further morphologies are obtained by considering the various deformation patterns described above. While the formation of the ETDs observed experimentally is largely dictated by kinetics, the thermodynamic stability of such structures can be analyzed by computing their formation energies, E_f . In the following, we describe a to-

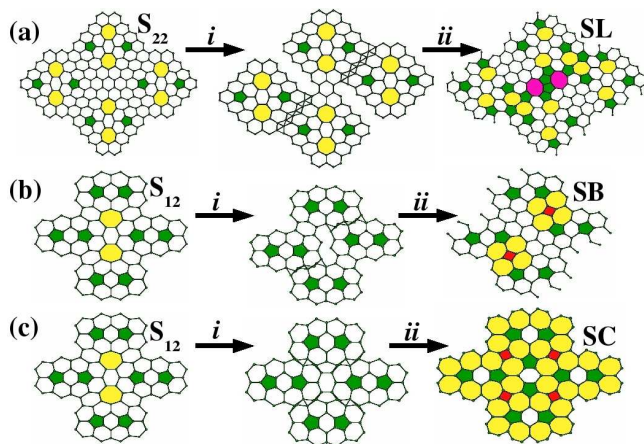


FIG. 4: Lowest-energy extended topological defects obtained from regeneration of holes and response to inhomogeneous deformations. Left column shows the parent geometry. Middle column shows imposed deformation. Right column shows resulting stress-free metastable ETD after full relaxation of internal atomic coordinates and cell vectors. (a) Pristine (without functionalization) showing clusters of 5-7 pairs as well as a 8558 unit. (b) Hydrogen-functionalized and (c) Hydroxyl-functionalized graphene show a morphological pattern where a tetragon is surrounded by four heptagons, with pentagons connected to its perimeter.

tal of 12 ETD configurations with $E_f \leq 0.30$ eV/atom. To put these formation energies in perspective, we quote the formation energy per atom of a fullerene molecule, 0.40 eV/atom with respect to a graphene sheet, and the energy of the pentaheptite, a theoretical allotrope of graphene composed entirely of pentagons and heptagons, 0.24 eV/atom,^{18,34} both computed with the same methodology as the ETDs energies in this work.

3. Formation energy and energetics

In the present study, the formation energies per atom of the structures without functionalization are defined as

$$E_f = \frac{E_{ETD}}{N} - \mu_C ; \quad (1)$$

where E_{ETD} is the *ab initio* total energy of the N -atom supercell containing the ETD and $\mu_C = E_{graphene}/N$ is the total energy per atom of an N -atom bulk graphene cell. For systems with hydrogen functionalization, we take graphane as reference, such that the formation energies per CH unit are defined as

$$E_f = \frac{E_{ETD+H}}{N} - (\mu_C + \mu_H) ; \quad (2)$$

where we keep μ_C as the energy per atom in graphene, and define $\mu_H = \mu_{CH} - \mu_C$, where $\mu_{CH} = E_{graphane}/N$ is the total energy per CH molecule for a bulk graphane calculation. For the hydroxyl-functionalized cases, we have:

$$E_f = \frac{E_{ETD+OH}}{N} - (\mu_C + \mu_{OH}) , \quad (3)$$

for the energy per COH unit, where again we keep μ_C as the energy per atom in graphene, and define $\mu_{OH} = \mu_{COH} - \mu_C$, where $\mu_{COH} = E_{graphenol}/N$ is the total energy per COH radical in a bulk graphenol calculation.

Table I shows the formation energies of the 12 ETDs, along with the energies of the parent geometries, S_{12} , S_{31} , and S_{22} , both with and without functionalization. In some cases, regeneration of holes did not take place, a feature that is consistent with the presence of holes in the final state of the RGO samples in Ref. 5. These are indicated in Table I as unreconstructed (UNREC.).

Figure 5(a) shows the six structures derived from deformed versions of the S_{12} geometry.¹⁸ From the figure, formation of pentagon-heptagons clusters is clearly the most common morphological patterns emerging from small-hole regeneration and relaxation of deformed graphene sheets, as found in recent experiments, but other morphologies are also manifest. We observe polygons ranging from tetragons to hendecagons, with color-coding indicated in the figure. The ETD in structure SA, with a nonagon connected to pentagons, is very similar to that present in the model of amorphous graphene

recently proposed as a high-specific area material for supercapacitor applications.³⁵ The five structures resulting from deformations of the S_{31} geometry are shown in Fig. 5(b). Linear polyacetylene-like chains are observed in the SG and SJ hydrogenated clusters, in structures with a strong sp^3 -hybridization content, which are stabilized by the functional groups. Such polymer-like carbon chains were also obtained in molecular dynamics models of RGO. Removal of functionalization in the SJ geometry leads to the recovery of a threefold connected network of pentagon-heptagon clusters, in the form of a climbed dislocation dipole, of the type observed in irradiated graphene samples.²³ Another striking geometry is the SI, which shows the presence of tetragons connected to decagons, with a reasonably low formation energy of 0.3 eV/atom when functionalized with hydrogens. Note the presence of a network of large pores, which would make defective graphene sheets with such morphologies candidates for applications as supercapacitors³⁵ and selective permeable membranes.^{36,37}

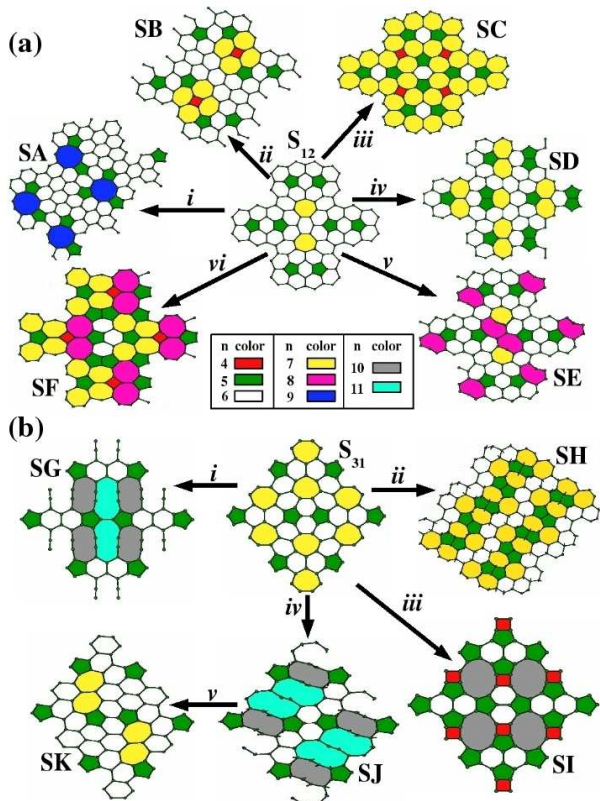


FIG. 5: (a) Low-energy extended topological defects derived from deformed versions of the S_{12} structure (shown in the center). (b) Low-energy extended topological defects derived from deformed versions of the S_{31} structure (shown in the center at the top row). Color coding for topological defects, ranging from tetragons to hendecagons, is indicated.

TABLE I: Formation energy E_f , in eV per formula unit, of extended topological defects in graphene. E_g is the electronic band gap in eV. Structures without functionalization are metallic, except the S_{31} . Functionalized structures are semiconductors or insulators, except the SE.

Structure	E_f		E_g	
	+H	+OH	+H	+OH
graphene	0.00	0.00	4.70	2.48
S_{12}	0.40	0.27	-	4.83
S_{22}	0.26	0.16	-	4.67
S_{31}	0.36	0.29	0.36	5.15
SA	0.27	0.22	UNREC.	4.97
SB	0.26	0.18	0.25	5.05
SC	0.37	0.21	0.20	5.20
SD	0.32	0.26	0.35	5.14
SE	0.43	0.30	0.29	*
SF	0.28	0.27	UNREC.	5.29
SG	0.59	0.32	0.22	0.82
SH	-	0.24	0.47	1.05
SI	0.40	0.30	0.41	1.30
SJ	-	0.34	0.28	2.71
SK	0.33	0.26	0.27	1.80
SL	0.24	-	-	-

4. Role of functionalization

Regarding the role of functionalization, we observe in Table I that the formation energy decreases with functionalization in all cases, with the exception of the hydroxyl-functionalized S_{31} , SD, and SI, which have slightly higher values of E_f than their pristine counterparts. For the hydrogen-functionalized ETDs, an average reduction of 95 meV/formula-unit is observed in Table I, while for the hydroxyl-functionalized ETDs, we obtain an average reduction of 125 meV/formula-unit. In both cases rather sizable maximum reductions of E_f of 0.27 and 0.37 eV/formula-unit occurs, respectively, for the H- and OH-functionalized SG morphologies, where functionalization leads to stabilization of polymer-like carbon chains. Functionalization also changes the electronic structure: while all pristine ETDs are metallic, with the exception of the S_{31} parent geometry, the functionalized ETDs are all semiconductors or insulators, with the exception of the SE. Table I shows the values of the gap for the semiconducting and insulating ETDs. This change in the electronic structure is connected with the incorporation of an sp^3 component in the electronic structure of these graphene materials, associated to the bonding of the functional groups to the graphene sheet.

III. CONCLUSION

In conclusion, *ab initio* calculations indicate that stress-relaxation of a graphene sheet containing topological defects may lead to the formation of extended topological defects showing morphological units that have been observed in recent experiments. We uncover the role of topological defects as a stress-accumulation site that induces the bond rotation events that generate the ETDs. Furthermore, we find that healing of small voids coupled with the relaxation of inhomogeneously strained regions also lead to the formation of ETDs, revealing a rich variety of morphological patterns and plastic deformation mechanisms in pure and functionalized graphene structures. Our results indicate that the tendency of de-

formed graphene sheets to form topological defect clusters is enhanced in the presence of functional groups, with a systematic reduction of the formation energies of such defective structures in graphane and in graphenol, when compared to graphene, in agreement with the available experimental evidence.

Acknowledgments

The authors acknowledge support from the Brazilian agencies CNPq, FAPEMIG, Rede de Pesquisa em Nanotubos de Carbono, INCT de Nanomateriais de Carbono, and Instituto do Milênio em Nanotecnologia-MCT.

-
- * Electronic address: rwnunes@fisica.ufmg.br
- ¹ A. H. C. Neto, F. Guinea, N. M. R. Peres, K. S. Novoselov, and A. K. Geim, *Rev. Mod. Phys.* **81**, 109 (2009), and references therein.
 - ² A. K. Geim and K. S. Novoselov, *Nature Mater.* **06**, 183 (2007).
 - ³ K. S. Novoselov, A. K. Geim, S. V. Morozov, D. Jiang, Y. Zhang, S. V. Dubonos, I. V. Grigorieva, and A. A. Firsov, *Science* **306**, 666 (2004).
 - ⁴ M. I. Katsnelson, K. S. Novoselov, and A. K. Geim, *Nature Phys.* **2**, 620 (2006).
 - ⁵ C. Gómez-Navarro, J. C. Meyer, R. S. Sudaram, A. Chuvilin, S. Kurasch, M. Burghard, K. Kern, and U. Kaiser, *Nano Lett.* **10**, 1144 (2010).
 - ⁶ J. Kotakoski, A. V. Krasheninnikov, U. Kaiser, and J. C. Meyer, *Phys. Rev. Lett* **106**, 105505 (2011).
 - ⁷ B. Westenfelder, J. C. Meyer, J. Biskupek, S. Kurasch, F. Scholz, C. E. Krill, and U. Kaiser, *Nano Lett.* **11**, 5123 (2011).
 - ⁸ A. Bagri, C. Mattevi, M. Acik, J. Y. Chabal, M. Chhowalla, and B. V. Shenoy, *Nature Chem.* **2**, 581 (2010).
 - ⁹ I. Jung, D. A. Dikin, R. D. Piner, and R. S. Ruoff, *Nano Lett.* **8**, 4283 (2008).
 - ¹⁰ S. Gilje, S. Han, W. Minsheng, L. W. Kang, and R. B. Kaner, *Nano Lett.* **7**, 3394 (2007).
 - ¹¹ C. Gomez-Navarro, R. T. Weitz, A. M. Bittner, M. Scolari, A. Mews, M. Burghard, and K. Kern, *Nano Lett.* **7**, 3499 (2007).
 - ¹² V. Lopez, R. S. Sundaram, C. Gomez-Navarro, D. Olea, M. Burghard, J. Gomez-Herrero, F. Zamora, and K. Kern, *Adv. Mater.* **21**, 4683 (2009).
 - ¹³ V. C. Tung, M. J. Allen, Y. Yang, and R. B. Kaner, *Nature Nanotechnol.* **4**, 2529 (2009).
 - ¹⁴ G. Eda, C. Mattevi, H. Yamaguchi, H. Kim, and M. Chhowalla, *J. Phys. Chem. C* **113**, 15768 (2009).
 - ¹⁵ X. Wu, M. Sprinkle, X. Li, F. Ming, C. Berger, and W. A. de Heer *Phys. Rev. Lett.* **101**, 026801 (2008).
 - ¹⁶ G. Eda, J. Ball, C. Mattevi, M. Acik, L. Artiglia, G. Granozzi, Y. Chabal, T. D. Anthopoulos, and M. Chhowalla, *J. Mater. Chem.* **21**, 11217 (2011).
 - ¹⁷ A. J. Stone and D. J. Wales, *Chem. Phys. Lett.* **128**, 501 (2011).
 - ¹⁸ J. daSilva-Araujo, H. Chacham, and R. W. Nunes, *Phys. Rev. B* **81**, 193405 (2010).
 - ¹⁹ W. Kohn and L. J. Sham, *Phys. Rev.* **140**, A1133 (1965).
 - ²⁰ L. Kleinman and D. M. Bylander, *Phys. Rev. Lett.* **48**, 1425 (1982).
 - ²¹ N. Troullier and J. L. Martins, *Phys. Rev. B* **43**, 1993 (1991).
 - ²² J. M. Soler, E. Artacho, J. D. Gale, A. Garcia, J. Junquera, P. Ordejon, and D. Sanchez-Portal, *J. Phys. Cond. Matt.* **14**, 2745 (2002).
 - ²³ J. C. Meyer, C. Kisielowski, R. Erni, M. D. Rossell, M. F. Crommie, and A. Zettl, *Nano Lett.* **8**, 3582 (2008).
 - ²⁴ F. Banhart, *Rep. Prog. Phys.* **62**, 1181 (1999).
 - ²⁵ C. Lee, X. Wei, J. W. Kysar, and J. Hone, *Science* **321**, 385 (2008).
 - ²⁶ E. Cadelano, P. L. Palla, S. Giordano, and L. Colombo, *Phys. Rev. Lett.* **102**, 235502 (2009).
 - ²⁷ K. Min and N. R. Aluru, *Appl. Phys. Lett.* **98**, 013113 (2011).
 - ²⁸ P. N. Keating, *Phys. Rev.* **152**, 774 (1966).
 - ²⁹ D. C. Elias, R. R. Nair, T. M. G. Mohiuddin, S. V. Morozov, P. Blake, M. P. Halsall, A. C. Ferrari, D. W. Boukhvalov, M. I. Katsnelson, A. K. Geim, and K. S. Novoselov, *Science* **323**, 610 (2009).
 - ³⁰ A. Lerf *et al.*, *J. Phys. Chem. B* **102**, 4477 (1998).
 - ³¹ M. U. Kahaly, S. P. Singh, and U. V. Waghmare, *Small* **4**, 2209 (2008).
 - ³² J. Lahiri, Y. Lin, P. Bozkurt, I. I. Oleynik, and M. Batzill, *Nature Nanotech.* **5**, 326 (2010).
 - ³³ S. S. Alexandre, A. D. Lúcio, A. H. C. Neto, and R. W. Nunes, arXiv:1109.6923 (2011).
 - ³⁴ V. H. Crespi, L. X. Benedict, M. L. Cohen, and S. G. Louie, *Phys. Rev. B* **53**, R13303 (1996).
 - ³⁵ Y. Zhu, S. Murali, M. D. Stoller, K. J. Ganesh, W. Cai, P. J. Ferreira, A. Pirkle, R. M. Wallace, K. A. Cychoz, M. Thommes, D. Su, E. A. Stach, and R. S. Ruoff, *Science* **332**, 1537 (2011).
 - ³⁶ J. Schrier, *J. Phys. Chem. Lett.* **1**, 2284 (2010).
 - ³⁷ D. E. Jiang, V. R. Cooper, and S. Dai, *Nano Lett.* **9**, 4019 (2009).